Available online at www.sciencedirect.com
ScienceDirect
Separation and Purification Technology 58 (2007) 68–75
Separation Purification Technology
www.elsevier.com/locate/seppur

Factors affecting nanofiltration performances in natural organic matter rejection and flux decline

Chalor Jarusutthirak [a,*], Supatpong Mattaraj [b], Ratana Jiraratananon [c]

[a] *Faculty of Science, King Mongkut's Institute of Technology Ladkrabang, Bangkok 10520, Thailand*
[b] *Department of Chemical Engineering, Faculty of Engineering, Ubon Rachathani University, Thailand*
[c] *Faculty of Engineering, King Mongkut's University of Technology Thonburi, Bangkok 10140, Thailand*

Abstract

A crossflow bench-scale test cell was used to investigate factors (i.e. NOM concentration, ionic strength, and solution pH) affecting natural organic matter (NOM) rejection and flux decline during nanofiltration (NF). Experimental results revealed that increased NOM concentration increased permeate flux decline, salt rejection, and NOM rejection, enhancing NOM accumulation on membrane surface. At high concentration of NOM, permeate flux curve corresponded to cake formation model. Increased ionic strength from 0.004 M to 0.1 M illustrated higher flux decline, possibly as a result of increasing osmotic pressure from higher concentration of salt. Solutions possessing high ionic strength (0.05 M) showed greater flux decline and NOM rejection than those having low ionic strength (0.01 M). Increased solution pH from 4 to 10 exhibited greater flux decline, caused by increasing salt rejection and enhancing salt concentration on membrane surface.

Keywords: Flux decline; Fouling; Nanofiltration; Natural organic matter; Permeate flux

1. Introduction

Natural organic matter (NOM) is naturally occurring and widely distributed throughout all aquatic environments containing in surface water [1]. NOM components consist of a heterogeneous mixture of complex organic materials, including humic substances (humic and fulvic acids), low molecular weight (hydrophilic) acids, proteins, carbohydrates, carboxylic acids, amino acids, and hydrocarbons [2]. Aquatic humic substances are colored, polyelectrolytic, organic acids isolated from water on XAD resins, nonvolatile and range in molecular weight from 500 to 5000 [1]. They play an important role as a precursor of disinfection by-products (DBPs) during chlorination process of water treatment [3]. The DBPs, e.g. trihalomethanes (THMs) and haloacetic acids (HAAs), possibly deteriorate human health due to their carcinogenic characters. Thus, a minimization of NOM as DBP-precursor is an alternative method to reduce potential adverse effects of the DBPs. Of particular interest is the use of nanofiltration (NF) membranes to control the formation of disinfection by-products (DBPs) by removing precursors, including dissolved natural organic matter (NOM). It has been reported that NF membrane is found to be effective in removal of NOM from surface water [4–7]. Typically, NF membrane has a molecular weight cutoff between 300 and 1000, while NF membrane operates at low pressure in the range of 344.6–1034 kPa (50–150 psi). Crossflow nanofiltration was investigated to reduce NOM fouling on membrane surface. Typical crossflow velocities in spiral-wound elements with mesh spacers range from 0.05 m s^{-1} to 1.5 m s^{-1} [8], similar to full-scale membrane operation. Membrane fouling can decrease permeate flux due to adsorption/deposition of solute on the membrane, accumulation of solute near the membrane surface, and gradual non-recoverable changes in cake formation. The main mechanisms of NOM fouling by NF membrane are described by size exclusion and electrostatic effects. However, the rejected NOM accumulation on membrane surface and/or in the membrane pores, causes membrane fouling, thus enhancing high operation and maintenance cost associated with membrane cleaning and replacement. Several investigators explained influencing factors causing membrane fouling, e.g. NOM concentration, feed water characteristics, inorganic scalants, and membrane properties [5–7,9].

The objectives of this study are to investigate factors (i.e. different NOM concentrations, ionic strength, and solution pH) affecting crossflow nanofiltration performances in natural

* Corresponding author. Tel.: +66 2326 4111x6245; fax: +66 2326 4415.
E-mail addresses: kjchalor@kmitl.ac.th (C. Jarusutthirak), mattas@ubu.ac.th (S. Mattaraj), ratana.jir@kmutt.ac.th (R. Jiraratananon).

1383-5866/$ – see front matter © 2007 Elsevier B.V. All rights reserved.
doi:10.1016/j.seppur.2007.07.010

Nomenclature

A_m	membrane area (m^2)
C_{bulk}	bulk concentration ($mg\,L^{-1}$)
J_v	permeate flux ($L\,m^{-2}\,h^{-1}$ or LMH)
J_0	initial permeate flux ($L\,m^{-2}\,h^{-1}$ or LMH)
J^*	permeate flux associated with the back-transport mass transfer ($L\,m^{-2}\,h^{-1}$ or LMH)
k	rate constant or fouling coefficient
k_A	kinetic rate constant for the pore blockage model (h^{-1})
k_B	kinetic rate constant for the pore constriction model ($m^{-0.5}\,h^{-0.5}$)
k_C	kinetic rate constant for the intermediate blocking model (m^{-1})
k_D	kinetic rate constant for the cake formation model ($h\,m^{-2}$)
n	dimensionless filtration constant
n_0	initial number of pores
P_f	operating pressure in feed (kPa)
P_p	operating pressure in permeate (kPa)
P_r	operating pressure in retentate (kPa)
R_c	the resistance of the polarization and cake (m^{-1})
$R_{f,NOM}$	feed rejection of NOM
$R_{f,s}$	feed rejection of salt
R_m	resistance due to membrane
$R_{r,NOM}$	retentate rejection of NOM
$R_{r,s}$	retentate rejection of salt
r_0	initial pore radius of membrane (m)
t	operating period (min)

Greek letters

α_{block}	pore blockage efficiency
α_{cake}	specific resistance of cake layer ($m\,mg^{-1}$)
α_{pore}	standard pore block efficiency
δ_c	depth of the particle cake (m)
δ_m	membrane thickness (m)
$\Delta\pi$	osmotic pressure ($=\pi_m - \pi_p$) (kPa)
σ	osmotic reflection coefficient

organic matter rejection and flux decline. A field reverse osmosis was used to separate organic matter from natural water source and further set up as a feed solution for NF experiments. A crossflow bench-scale test cell was used to determine NF performances during filtration experiments. Mathematical models were used to interpret membrane performances of NF membrane. Finally, an integrated understanding of NOM rejection and membrane fouling during NF membrane leads to efficient operations of NF processes.

2. Theoretical basis

Mathematical models have been illustrated to explain permeate flux decline in the dead-end operation during filtration [10–12]. The mathematical models can be shown as follows

$$\frac{dJ_v}{dt} = -kJ_v(J_v)^{2-n} \quad (1)$$

where k is a rate constant or fouling coefficient and n is the dimensionless filtration constant: (1) cake formation model corresponds to $n = 0$, (2) intermediate blocking model corresponds to $n = 1$, (3) pore constriction or standard blocking model corresponds to $n = 1.5$, and (4) complete pore blocking corresponds to $n = 2.0$.

For a crossflow membrane system, the additional term (J^*) is included in the mathematical fouling models expressed by Field et al. [12]. The mathematical models can be illustrated in the following equations [6]:

- Type I. Pore blocking model (or complete pore blocking model):

  The rate of change in the number of open pores is assumed to be proportional to the rate of particle convection to the membrane surface:

$$\frac{dJ_v}{dt} = -\frac{\alpha_{block}A_mC_{bulk}J_0}{n_0}(J_v - J^*) = -k_A(J_v - J^*) \quad (2)$$

  where α_{block} is the pore blockage efficiency, A_m the membrane area (m^2), C_{bulk} the bulk concentration ($mg\,L^{-1}$), J_v the permeate flux ($L\,m^{-2}\,h^{-1}$), J_0 the initial permeate flux ($L\,m^{-2}\,h^{-1}$), J^* the permeate flux associated with the back-transport mass transfer ($L\,m^{-2}\,h^{-1}$), t the operating period (min), n_0 the initial number of pores, and k_A is the kinetic rate constant for the pore blockage model (min^{-1}).
- Type II. Pore constriction model (or standard blocking model):

  The rate of change in the pore volume is assumed to relate to the rate of particle convection to the membrane surface:

$$\frac{dJ_v}{dt} = -\frac{(2\alpha_{pore}A_mC_{bulk}J_0)^{0.5}}{\pi r_0^2\delta_m}J_v^{0.5}(J_v - J^*) = -k_BJ_v^{0.5}(J_v - J^*) \quad (3)$$

  where α_{pore} is the standard pore block efficiency, δ_m the membrane thickness (m), r_0 the initial pore radius of membrane (m), and k_B is the kinetic rate constant for the pore constriction model ($LMH^{-0.5}\,min^{-1}$ or $m^{-0.5}\,min^{-0.5}$).
- Type III. Intermediate blocking model:

  The rate of change in the cake thickness (limit on the membrane surface) is assumed to relate with the rate of particle convection to the membrane surface:

$$\frac{dJ_v}{dt} = -\frac{\alpha_{cake}R_c}{(R_m + R_c)\delta_c}A_mC_{bulk}J_v(J_v - J^*) = -k_CJ_v(J_v - J^*) \quad (4)$$

  where δ_c is the depth of the particle cake (m), α_{cake} the specific resistance of cake layer ($m\,mg^{-1}$), R_m is the resistance due to membrane, R_c the resistance of the polarization and cake (m^{-1}), and k_C is the kinetic rate constant for the intermediate blocking model ($LMH^{-1}\,min^{-1}$ or m^{-1}).

- Type IV. Cake formation model:

  The hydraulic resistance caused by the particle cake is assumed to be proportional to the cake mass, m_{cake}:

$$\frac{dJ_v}{dt} = -\frac{\alpha_{cake} C_{bulk}}{R_m J_0} J_v^2 (J_v - J^*) = -k_D J_v^2 (J_v - J^*) \quad (5)$$

  where α_{cake} is the specific resistance of cake layer ($m\,mg^{-1}$) and k_D is the kinetic rate constant for the cake formation model ($LMH^{-2}\,min^{-1}$ or $min\,m^{-2}$).

3. Experimental

3.1. Natural water

Natural water was taken from water reservoir at Ubon Ratchathani's University (UBU), Thailand, which served as water supply in UBU community. Natural water consists of total organic carbon (TOC) and $UV_{254\,nm}$ at about 4.54 mg L^{-1} and 0.185 cm^{-1}, respectively. Specific ultraviolet absorbance (SUVA), determined by the ratio between $UV_{254\,nm}$ and TOC, was approximately 4.07 L $mg^{-1}\,m^{-1}$. The natural water used was softwater as its low conductivity and hardness (31.9 μS cm^{-1} (at 25 °C) and 15.4 mg L^{-1} as $CaCO_3$, respectively).

3.2. Natural organic matter

Natural organic matter (NOM) was isolated using a field reverse osmosis (RO) system. The procedure was recently studied by Kilduff et al. [13]. This RO was a polyamide thin-film composite (TFC) RO membrane (model AG4040F-spiral-wound crossflow, GE Osmonics Inc., USA), which provides high performance for concentrating NOM. Field RO system consists of pretreatment (i.e. sand filtration, 5-μm polypropylene (PP) and 1-μm PP cartridge prefilter in series with a sodium-form cation exchange softener) to remove multivalent cations (Ca^{2+} and Mg^{2+}), and followed by 1-μm and 0.45-μm PP cartridge filters. The pretreated water was subsequently transferred to a 150-L stainless steel drum as a sample reservoir. The pretreated water was then pumped by a transfer pump (model PL-95 M, Bomba-Elias, Bacelona, Spain) through the RO system while a high-pressure stainless steel multi-stage vertical centrifugal pump (Model CRN3-25, GRUNDFOS), was used to isolate NOM from the pretreated water. A back pressure valve was used to adjust the operating pressures ranging from 554.9 kPa to 1413 kPa (80.5–205 psi). The pretreated water was used about 1000 L while the concentrated water was collected with a concentration of factor about 28–30. The final concentrated NOM solution in the sample reservoir was collected after system cleaning and kept in a refrigerator (4 °C) to minimize microbial activity.

3.3. Nanofiltration membrane

Thin-film polysulfone nanofiltration membrane, obtained from GE Osmonics, Inc., was used to investigate NF performance on membrane surface. This membrane model is the HL 2540F1072 (series 7933937). According to the manufacturer's information, the membrane has a molecular weight cutoff (MWCO) of 150–300 Da, determined with glucose and sucrose compounds. The operating pH was in the range of 3.0–9.0 while the cleaning pH was in the range of 1.0–10.0. Low chlorine resistance was about 0.1 ppm. The maximum operating temperature was about 50 °C. The nanofiltration sheets were stored in 1% $Na_2S_2O_5$ and kept in 4 °C to minimize bacterial activity.

3.4. Crossflow nanofiltration experiment using crossflow bench-scale test cell

Fig. 1 shows the schematic diagram of bench-scale crossflow nanofiltration experimental set-up with recycle loop. The system consists of a stainless steel test cell (SEPA, Osmonics) that houses a single membrane sheet of 0.014 m^2 with a maximum operating pressure of 1000 psi. A high-pressure stainless steel piston feed pump (30 mL min^{-1} @ 3000 psi, Eldex, Model CC-100-S-4, Napa, CA, USA) was used for membrane operating pressures while a high capacity booster recycle pump (Gear pump, Model 75211-35, Cole-Parmer Instrument, Co., Vernon Hills, IL, USA) was used to adjust a high crossflow velocity in the recycle loop. Hydraulic hand pump was used to hold the system pressure at the top of bench-scale test

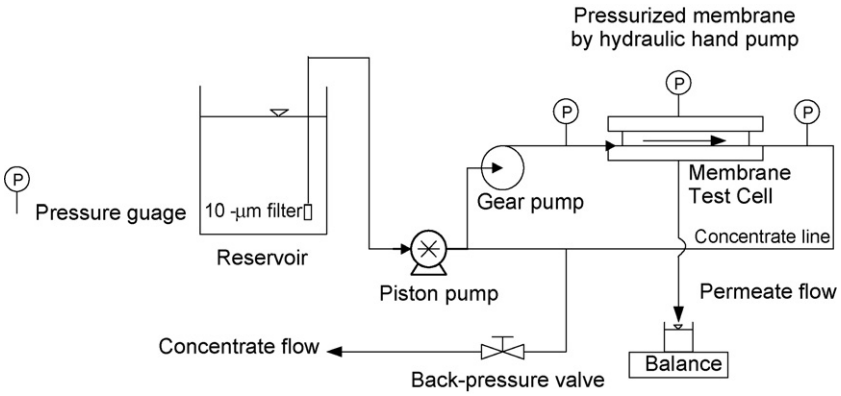

Fig. 1. Bench-scale crossflow nanofiltration experimental set-up.

cell. Mesh feed spacer was used to create hydrodynamic flow conditions similar to that employed in full-scale spiral-wound elements. Inlet temperature was approximately 25 °C and kept constant throughout filtration experiments. Recovery was operated at 85% during filtration experiments, and crossflow velocity of 0.1 m s^{-1} (similar to that of full-scale membrane) corresponding to a flowrate of 530 mL min^{-1} in the recycle loop [8].

3.5. Filtration experiments

Filtration procedure was basically followed with Jarusutthirak et al. [6]. Membrane NF sheets were rinsed with cleaned DI water and then transferred to the bench-scale test cell. The membrane sheets were then cleaned with citric acid solution of pH 3–4, and followed with sodium hydroxide solution of pH 10 for 30 min each. Cleaned water flux was determined with a function of transmembrane pressure. Cleaned DI water was subsequently tested for 30-min membrane compaction with an initial water flux of 45 LMH (L m^{-2} h^{-1}). Cleaned water flux was subsequently determined with increased operating pressure before NOM solution was used with the system. Feed NOM solutions were prepared for each tested condition. Prior to NOM filtration, a 200–300 mL NOM solution was initially used to flush the bench-scale system. NOM solution was then filtered through the NF membrane. The piston feed pump was subsequently adjusted in order to achieve an initial permeate flux of 45 LMH with 85% recovery. The transmembrane pressure was recorded and kept constant during filtration experiment. Permeate and retentate flow was periodically measured using analytical balance (Model BL-2200H, Shimadzu, Japan) in order to calculate permeate flux and recovery throughout filtration experiments. Permeate and retentate samples were conducted to determine NOM and conductivity rejection. After filtration was terminated, two steps of cleaning, i.e. hydrodynamic cleaning followed by chemical cleaning, were performed; First, for hydrodynamic cleaning, DI water was recirculated in the recycle loop for 30 min with a crossflow velocity of 0.25 m s^{-1}, which was higher than that during operation. For chemical cleaning, alkaline solution (using NaOH) with pH of 10, was first used to recirculate in the system, and followed with acidic solution (using HCl) with pH of 3 at a crossflow velocity of 0.25 m s^{-1} for 30 min each. After each cleaning, water fluxes at different operating pressures were measured to determine water flux recovery.

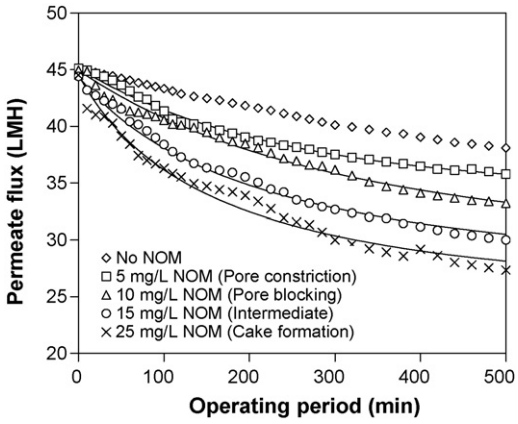

Fig. 2. Influence of NOM concentrations on permeate flux.

4. Results and discussion

4.1. Influence of NOM concentration on NOM rejection and flux decline

Fig. 2 shows the influence of NOM concentration on permeate flux. NOM concentrations were varied from 0 mg L^{-1} to 25 mg L^{-1} with constant solution pH of 7 and ionic strength of 0.01 M NaCl (1170 μS cm^{-1} at 25 °C). Dot points were the experimental data while solid lines were fitted well with fouling mathematical models. Table 1 shows the model parameters obtained from mathematical models on different NOM concentrations.

It was observed that as NOM concentrations increased from 0 mg L^{-1} to 25 mg L^{-1}, permeate flux decline became more significant. Normalized permeate flux (t = 8 h) decreased from 0.85 to 0.61 as NOM concentration increased from 0 mg L^{-1} to 25 mg L^{-1}. In the absence of NOM, permeate flux decreased during filtration experiment as a result of increased osmotic pressure from salt concentration (i.e. ionic strength of 0.01 M NaCl). This can be explained by the following equation:

$$J_v = L_p(\Delta P - \sigma\Delta\pi) = \frac{Q_p}{A_m} \quad (6)$$

where ΔP is the average transmembrane pressure ($(P_f + P_r)/2 - P_p$) (kPa), L_p the membrane permeability (L m^{-2} h^{-1} kPa^{-1} or LMH kPa^{-1}), σ the osmotic reflection coefficient ($=(1 - C_p)/C_m$), $\Delta\pi$ the osmotic pressure ($=\pi_m - \pi_p$) (kPa), and A_m is the effective membrane area (m^2).

Table 1
Model parameters from mathematical models on different NOM concentrations

Concentration (mg L^{-1})	Model parameter											
	Pore blocking			Pore constriction			Intermediate			Cake formation		
	k_A (h^{-1})	J^* (LMH)	SSE	k_B ($m^{-0.5}$ $h^{-0.5}$)	J^* (LMH)	SSE	k_C (m^{-1})	J^* (LMH)	SSE	k_D (h m^{-2})	J^* (LMH)	SSE
5	0.294	35.4	2.803	1.205	34.3	2.359	6	34.3	2.615	114	32.7	2.785
10	0.246	32.3	5.31	0.968	30.2	5.756	4.5	29.5	5.41	108	29	5.474
15	0.309	29.7	1.816	1.275	27.8	1.761	5.88	26.8	1.635	167.4	27.4	5.356
25	0.397	28.1	17.707	1.729	26.6	18.426	8.7	26.3	16.355	221.4	25.6	15.186

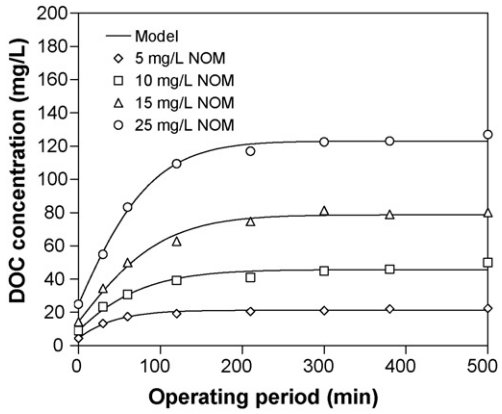

Fig. 3. NOM concentration in retentate during NF operation at different initial concentrations of NOM.

From Eq. (6), at a constant operating pressure, the increase of osmotic pressure by NaCl could decrease permeate flux. In addition, it was reported that the flux decline of solutions having NaCl alone was caused by an increased osmotic effect, while increasing flux decline of feed solution containing both salt and NOM resulted from a combination of resistance from an NOM deposition and an increasing osmotic effect [5]. The increase of NOM concentration caused higher flux decline. At NOM concentration of 25 mg L^{-1}, permeate flux showed the greatest flux reduction. According to membrane fouling model, increased NOM concentrations from 5 mg L^{-1} to 25 mg L^{-1} changed fouling mechanisms from pore blocking/pore constriction model (at low NOM concentration) to cake formation model (at high NOM concentration). Model parameters, permeate flux associated with the back-transport mass transfer (J^*) and kinetic rate constants, were obtained from minimizing sum squared error (SSE) between experimental data and mathematical models. The overall model parameters were tabulated in Table 1. Solutions having high NOM concentration decreased permeate flux during filtration. This was caused by increased NOM accumulation, suggesting increased cake formation on the membrane surface.

Fig. 3 exhibits the increasing NOM concentration introduced to membrane during the filtration processes while the process performances of NF membrane, in terms of NOM rejection, at different NOM concentrations were tabulated in Table 2. The equation was used to calculate steady-state retentate concentration for NOM ($C_{ss,NOM}$) and salt ($C_{ss,s}$) based on overall mass balance reported by Kilduff et al. [5]. At 25-mg L^{-1} NOM, the feed rejection ($R_{f,NOM}$) and retentate rejection of NOM ($R_{r,NOM}$) exhibited the highest value about 88.4% and 97.6%, respectively. It was evident that increased NOM concentration increased feed rejection of NOM from 75.3% to 88.4% while NOM rejections based on retentate were relatively high from 94.9% to 97.6%. At 25-mg L^{-1} NOM concentration, the average feed rejection shows the highest NOM rejection, indicating an increased NOM accumulation on the membrane surface. In addition, permeate flux curve corresponded with cake formation model, suggesting increased NOM mass deposited on the membrane surface. The steady-state NOM concentration of 25-mg L^{-1} NOM concentration was approximately 122.1 mg L^{-1}. With increased NOM concentration from 0 mg L^{-1} to 25 mg L^{-1}, the rejections of salt in the feed and retentate line increased in the range of 3.51–5.7% and 21.4–28.2%, respectively. This indicated a relatively low rejection of salt concentration when compared with an aromatic polyamide thin-film composite membrane (NF-70, Dow-FilmTec, Minneapolis, MN) at the same condition studied by Kilduff et al. [5]. They reported that the feed salt rejection ranged from 46.3% to 72.7% with an increased NOM concentration from 0 mg L^{-1} to 25 mg L^{-1}. They also indicated an increased with osmotic effect due to the presence of NOM, thus increased salt rejection by the result of electrostatic repulsion between Cl^- ions and charged functional groups on the NOM molecules. However, in the absence of NOM, the salt rejection can be caused by electrostatic repulsion between Cl^- ions and negatively charged NF membrane. This may affect NF membrane pores while the results were confirmed by pore blocking model. These experimental results fitted relatively well with the pore blocking model in the absence of NOM concentration.

Table 2
Process performance of NF membrane caused by NOM concentration

Parameters	NOM concentration (mg L^{-1})				
	0	5	10	15	25
$C_{p,NOM}$ (mg L^{-1})	–	1.08	1.93	3.2	2.9
$C_{ss,NOM}$ (mg L^{-1})	–	21.2	45.5	79.06	122.1
$C_{p,s}$ (mol L^{-1})	0.011	0.0105	0.0104	0.0103	0.0102
$C_{ss,s}$ (mol L^{-1})	0.014	0.01426	0.01392	0.0138	0.0142
$R_{f,NOM}$ (%)	–	75.3	78.5	77.7	88.4
$R_{r,NOM}$ (%)	–	94.9	95.8	95.9	97.6
$R_{f,s}$ (%) (salt)	3.51	4.3	5.4	4.6	5.7
$R_{r,s}$ (%) (salt)	21.4	26.3	25.3	25.4	28.2

4.2. Influence of ionic strength on permeate flux

Fig. 4 presents the influence of ionic strength on permeate flux. Solutions contained no NOM and pH of 7, while ionic strength concentrations were varied from 0.004 M to 0.1 M NaCl. Experimental results showed that increased ionic strength from 0.004 M to 0.1 M NaCl decreased permeate flux curve, These indicated an increased salt concentration on membrane

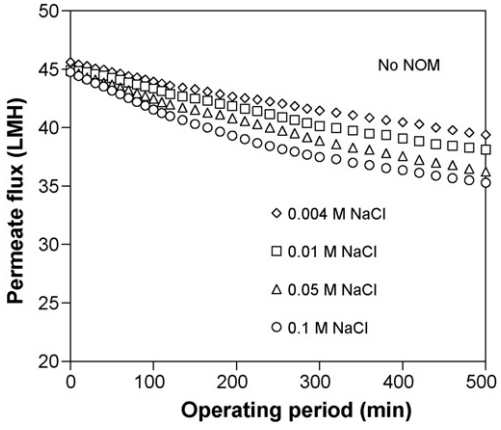

Fig. 4. Influence of ionic strength in the absence of NOM on permeate flux.

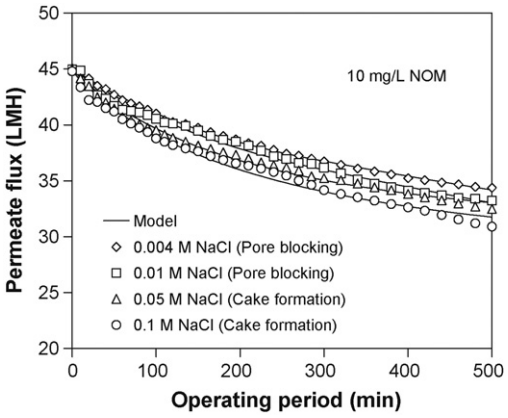

Fig. 5. Influence of ionic strength in the presence of NOM on permeate flux.

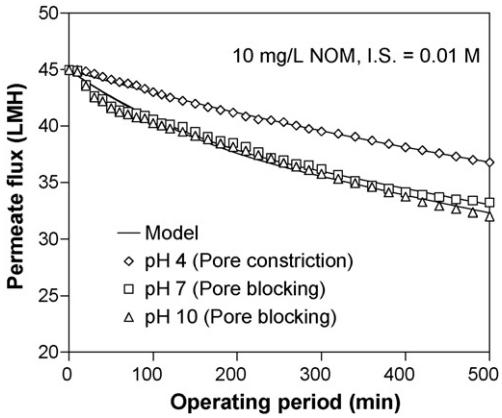

Fig. 6. Influence of pH on permeate flux for ionic strength of 0.01 M NaCl.

surface, which can decrease permeate volume passing through the NF membrane surface. Increased ionic strength can reduce charge repulsion caused by charge interaction between positively charged Na^+ and negatively charged NF membrane, thus enhancing a reduction of permeates flux and salt rejection. These phenomena can also be explained by the effect of increasing osmotic pressure in the system with higher concentration of NaCl salt. Braghetta et al. [14] found that membrane fouling increased by decreasing pH and increasing ionic strength.

In the presence of 10-mg L^{-1} NOM, permeate flux curves were investigated by varying ionic strengths from 0.004 M to 0.1 M NaCl. Fig. 5 shows the effect of ionic strength in the presence of NOM on permeate flux. Table 3 presents the model parameters on ionic strength in the presence of NOM. It was observed that increased ionic strength slightly increased permeate flux decline. At low ionic strength (0.004 M and 0.01 M NaCl), the permeate flux curves were fitted with pore blocking model based on minimized sum squared error. This suggests that charge interaction between positively charged Na^+ and negatively charged NF membrane dominates permeate flux decline. However, the permeate flux curves with high ionic strength (0.05 M and 0.1 M NaCl) were fitted relatively well with cake formation model. This indicates the charge interaction between positively charged Na^+ and negatively charged NOM functional groups, causing NOM accumulation on the membrane surface. Braghetta et al. [15] indicated that NOM accumulation increased with high ionic strength, suggesting a reduction of charge repulsion and increased potential build-up on the membrane surface.

From Table 3, the kinetic rate constants for pore blocking (k_A) of 0.004 M and 0.01 M NaCl were approximately 0.263 h^{-1} and 0.246 h^{-1}, while the minimum SSEs were about 0.516 and 5.31, respectively. The kinetic rate constants for cake formation model (k_D) of 0.05 M and 0.1 M NaCl were about 156 h m^{-2} and 150 h m^{-2}, while the minimum SSEs were 3.693 and 7.06, respectively.

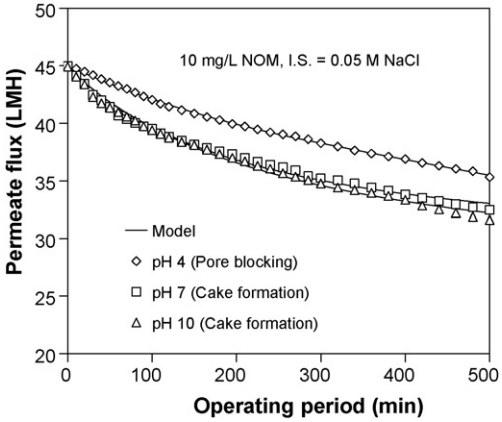

Fig. 7. Influence of pH on permeate flux for ionic strength of 0.05 M NaCl.

4.3. Influence of pH on permeate flux

Solution pH can influence permeate flux and rejection. Figs. 6 and 7 show the influence of pH on permeate flux for ionic strength of 0.01 M and 0.05 M NaCl, respectively. Dot points were the experimental data while solid lines were followed with mathematical models. Table 4 presents model parameters affected by solution pH. At low ionic strength of

Table 3
Model parameters on ionic strength in the presence of NOM

Concentration	Model parameter											
	Pore blocking			Pore constriction			Intermediate			Cake formation		
	k_A (h^{-1})	J^* (LMH)	SSE	k_B ($m^{-0.5}\,h^{-0.5}$)	J^* (LMH)	SSE	k_C (m^{-1})	J^* (LMH)	SSE	k_D (h m^{-2})	J^* (LMH)	SSE
0.004 M NaCl	0.263	33.7	0.516	1.055	32.1	0.659	5.52	32.4	0.951	120	31.4	0.977
0.01 M NaCl	0.246	32.3	5.31	0.968	30.2	5.756	4.5	29.5	5.41	108	29	5.474
0.05 M NaCl	0.355	33.1	3.895	1.5	32	5.683	7.08	31.6	4.906	156	30.6	3.693
0.1 M NaCl	0.325	31.5	7.327	1.35	30	9.466	6.54	29.6	8.443	150	28.6	7.06

Table 4
Model parameters affected by solution pH

Ionic strength	Model parameter											
	Pore blocking			Pore constriction			Intermediate			Cake formation		
	k_A (h^{-1})	J^* (LMH)	SSE	k_B ($m^{-0.5}\,h^{-0.5}$)	J^* (LMH)	SSE	k_C (m^{-1})	J^* (LMH)	SSE	k_D ($h\,m^{-2}$)	J^* (LMH)	SSE
I.S. = 0.01 M												
pH 4	0.069	26.8	0.726	0.238	20.2	0.678	1.5	24.9	1.085	31.2	22.4	1.613
pH 7	0.246	32.3	5.31	0.968	30.2	5.756	4.5	29.5	5.41	108	29	5.474
pH 10	0.232	31.2	6.456	0.892	28.7	7.992	4.02	27.5	7.437	79.2	24.3	6.615
I.S. = 0.05 M												
pH 4	0.171	33.3	0.263	0.637	30.7	0.489	2.76	29.3	0.455	50.7	25.6	0.412
pH 7	0.355	33.1	3.895	1.5	32	5.683	7.08	31.6	4.906	156	30.6	3.693
pH 10	0.317	32	3.41	1.308	30.5	5.135	6.12	29.9	4.406	132	28.42	3.317

0.01 M, increased solution pH from 4 to 7 increased permeate flux decline. The retentate rejections of salt were determined in the range of 16.0%, 25.5%, and 37.3% with increased solution pH of 4, 7, and 10, respectively. Solutions having high solution pH of 7 and 10 showed greater salt rejection than those having low solution pH. This indicated that increased salt rejection increased permeate flux decline, suggesting increased charge repulsion between negatively charged NF membrane and functional groups in the NOM molecules for high solution pH. Kilduff et al. [5] reported that the effect of pH on solution rejection was an important factor on permeate flux decline compared with the effect of membrane permeability.

Solutions having solution pH of 4 exhibited relatively low rejection. This can be affected by charge interaction between positively charged H^+ and negatively charged NF membrane, allowing salt passage through the NF membrane surface, and decreasing salt rejection. Based on fitting mathematical models, permeate flux curves were correlated with pore constriction and pore blocking model. It was observed that the retentate rejections of NOM were approximately 91.6–94.9%, indicating relatively low rejections compared with those of high ionic strength of 0.05 M. From Table 4, the kinetic rate constants of fouling mechanisms for solution pH 4, 7, and 10 were about 0.238 $(m\,h)^{-1/2}$ (k_B, pore constriction), 0.246 h^{-1} (k_A, pore blocking), and 0.232 h^{-1}(k_A, pore blocking), respectively.

At high ionic strength of 0.05 M NaCl, increased solution pH from 4 to 10 showed similar trend for permeate flux curve of low ionic strength of 0.01 M NaCl. The permeate flux curve of pH 7 and 10 exhibited the greatest permeate flux reduction. However, permeate flux curves of pH 7 and 10 show no significant difference. The retentate rejections of salt were 17.9%, 15.9%, and 26.1% with increasing solution pH of 4, 7, and 10, respectively. At low solution pH of 4, permeate flux curves were related to pore blocking model, while permeate flux curves were related to cake formation model at solution pH of 7 and 10. The retentate rejections of NOM were approximately 95.3–96.4% with increasing solution pH from 4 to 10. This suggests that high ionic strengths (0.05 M NaCl) can dominate permeate flux curve compared with the effect of solution pH on salt rejection. Permeate flux decline can be caused by reduced charge repulsion between positively charged Na^+ and functional groups in the NOM molecules, thus increased NOM accumulation on the membrane surface. This was confirmed by permeate flux curves, which correspond to cake formation model for solution pH of 7 and 10. From Table 4, the kinetic rate constants of fouling mechanisms for solution pH 4, 7, and 10 were about 0.171 h^{-1} (k_A, pore blocking), 156 $h\,m^{-2}$ (k_D, cake formation), and 132 $h\,m^{-2}$ (k_D, cake formation), respectively.

Salt rejection can affect permeate flux curve. Solutions having high solution pH of 7 and 10 showed greater salt rejection than those having low solution pH. Solution pH of 4 exhibited less permeate flux decline than solution pH of 7 and 10. These were observed for both low and high ionic strengths. Solutions having low solution pH of 4 and high ionic strength can affect membrane surface, reducing charge repulsion between positively charged Na^+ and H^+ and negatively charged NF membrane. This allows an increased salt passage through the NF membrane surface, thus decreased salt rejection and permeate flux decline.

5. Conclusions

Performances of nanofiltration membrane in terms of NOM rejection and permeate flux decline were influenced by NOM concentration, ionic strength, and solution pH. Mathematical fouling models were used to evaluate fouling mechanisms on the membrane surface. The increase of NOM concentration from 0 mg L^{-1} to 25 mg L^{-1} caused higher NOM rejection, membrane fouling, and greater flux decline, as a result of NOM accumulation on membrane surface. From low to high NOM concentration, fouling mechanisms exhibited a change of fouling patterns from pore blocking and pore constriction model (low NOM concentration) to cake formation model (high NOM concentration). In the absence of NOM, increased ionic strength from 0.004 M to 0.1 M decreased permeate flux, caused by osmotic effect of feed solutions. In the presence of NOM, feed solutions possessing high ionic strength of 0.05 M NaCl showed greater flux decline than those with low ionic strength of 0.01 M NaCl, possibly indicated by a combination of resistance from NOM accumulation and osmotic effects. The experimental results were corresponded with cake formation model. The increase of solution pH from 4 to 10 showed greater flux decline, affected by increased salt concentrations on membrane surface and/or pores. These results were related with pore blocking and pore constriction model.

Acknowledgements

The authors would like to thank the Thailand Research Fund (TRF) and the Commission on Higher Education, Thailand, for financial support. We also would like to thank the Department of Chemical Engineering, Faculty of Engineering, Ubon Rachathani University, Thailand, for all equipments applied in this research.

References

[1] E.M. Thurman, Organic GeoChemistry of Natural Waters, Martinus Nijhoff/Dr. W. Junk Publishers, Dordrecht, 1985.
[2] E. Tipping, Cation binding by humic substances, Cambridge Environmental Chemistry Series, 1948, ISBN 0 521 62146 1.
[3] S.W. Krasner, M.J. McGuire, J.G. Jacangelo, N.L. Patania, K.M. Reagan, E.M. Aieta, The occurrence of disinfection by-products in US drinking water, J. AWWA 81 (8) (1989) 41–53.
[4] P. Fu, H. Ruiz, K. Thompson, C. Spangenberg, Selecting membranes for removing NOM and DBP precursors, J. AWWA 86 (12) (1994) 55–72.
[5] J.E. Kilduff, S. Mattaraj, G. Belfort, Flux decline during nanofiltration of naturally-occurring dissolved organic matter: effects of osmotic pressure, membrane permeability, and cake formation, J. Membr. Sci. 239 (1) (2004) 39–53.
[6] C. Jarusutthirak, S. Mattaraj, R. Jiraratananon, Influence of inorganic scalants and natural organic matter on nanofiltration membrane fouling, J. Membr. Sci. 287 (2007) 138–145.
[7] S. Hong, M. Elimelech, Chemical and physical aspects of natural organic matter (NOM) fouling of nanofiltration membranes, J. Membr. Sci. 132 (1997) 159–181.
[8] S.C. Allgeier, R.S. Summers, Evaluating NF for DBP control with the RBSMT, J. AWWA 87 (3) (1995) 87–99.
[9] M. Mattari, L. Puro, J. Nuortila-Jokinen, M. Nystrom, Fouling effects of polysaccharides and humic acid in nanofiltration, J. Membr. Sci. 165 (2000) 1–17.
[10] J. Hermia, Constant pressure blocking filtration laws: application to power-law non-newtonian fluids, Trans. Inst. Chem. Eng. 60 (1982) 183–187.
[11] C.-C. Ho, A.L. Zydney, A combined pore blockage and cake filtration model for protein fouling during microfiltration, J. Membr. Sci. 232 (2000) 389–399.
[12] R.W. Field, D. Wu, J.A. Howell, B.B. Gupta, Critical flux concept for microfiltration fouling, J. Membr. Sci. 100 (1995) 259–272.
[13] J.E. Kilduff, S. Mattaraj, A. Wigton, M. Kitis, T. Karanfil, Effects of reverse osmosis isolation on reactivity of naturally occurring dissolved organic matter in physicochemical processes, Water Res. 38 (4) (2004) 1026–1036.
[14] A. Braghetta, F.A. DiGiano, W.P. Ball, Nanofiltration of natural organic matter: pH and ionic strength effects, J. Environ. Eng. 123 (7) (1997) 628–641.
[15] A. Braghetta, F.A. DiGiano, W.P. Ball, NOM accumulation at NF membrane surface: impact of chemistry and shear, J. Environ. Eng. 124 (11) (1998) 1087–1098.